

UNIVERSITÀ DEGLI STUDI DI CATANIA
DIPARTIMENTO DI INGEGNERIA ELETTRICA, ELETTRONICA ED
INFORMATICA

DOTTORATO DI RICERCA IN INGEGNERIA INFORMATICA E DELLE
TELECOMUNICAZIONI
XXVII CICLO

GREEN SOLUTIONS FOR LTE-A MOBILE NETWORKS

ING. ANNA DUDNIKOVA

Coordinatore
Chiar.ma Prof.ssa V. CARCHIOLO

Tutor
Chiar.ma Prof.ssa D. PANNO

to my family

CONTENTS

| | | |
|----------|-----------------------------------------------------------|-----------|
| 1 | Introduction and Structure of the dissertation | 3 |
| 1.1 | Introduction | 3 |
| 1.2 | Structure of this Dissertation | 5 |
| 2 | Motivation and Related Work | 7 |
| 2.1 | Overview on Femtocell Technology | 7 |
| 2.2 | Technical challenges that arise with femtocell deployment | 10 |
| 2.3 | Overview on Related Works | 11 |
| 3 | Pilot Power Control Approach | 17 |
| 3.1 | Problem Formulation | 17 |
| 3.2 | Network Model | 18 |
| 3.3 | Algorithm Description | 20 |
| 3.3.1 | Listen Mode | 21 |
| 3.3.2 | Initial Power Setting | 22 |
| 3.3.3 | Dynamic Power Adaption | 23 |
| 3.3.4 | Stabilization State | 27 |

| | | |
|----------|--------------------------------------------------------|-----------|
| 4 | Performance Evaluation | 31 |
| 4.1 | Simulation assumptions and performance metrics . . . | 32 |
| 4.2 | Determination of thresholds | 33 |
| 4.3 | Evaluation of scalability and robustness | 36 |
| 4.4 | Evaluation of Stability | 42 |
| 4.5 | Evaluation of Energy Efficiency | 45 |
| 4.6 | Multi-MBS environment | 51 |
| 4.6.1 | <i>NOISE_UL</i> estimation in multi-MBS scenario | 52 |
| 4.6.2 | <i>wSINR</i> estimation in multi-MBS scenario . . . | 52 |
| 5 | Implementation issues | 55 |
| 5.1 | Network Listen Mode | 55 |
| 5.2 | SINR | 56 |
| 6 | Appendix | 59 |
| 6.1 | The noise level on the uplink frequency band | 59 |
| 6.2 | Wideband Signal to Interference plus Noise Ratio . . . | 61 |
| 6.3 | Simulation parameters | 63 |
| 7 | Conclusions | 65 |
| 7.1 | Concluding remarks | 65 |
| 7.2 | Possible work extensions. | 67 |
| 7.2.1 | Hybrid Access mode for Femtocells. | 67 |
| 7.2.2 | Automation of setting of thresholds' values. . . | 67 |
| 7.3 | List of Publications | 68 |

Acknowledgements

First of all, I want to thank my supervisor, Prof. Daniela Panno. Thanks for all the support over the last three years, for advices, patience, for being always ready to help. I consider it a privilege to have been working under your guidance.

I sincerely thank Antonio Mastrosimone who, in the course of the last year of my PhD program, is my friend, colleague and office mate that became an integral part of my workdays. Thank you for your contributions to this dissertation and all the support.

I would like to thank also all my colleagues (Giuseppe la Torre, Salvatore Monteleone, Gaetano Carmelo la Delfa, Daniela Ventura and others). Thanks for being always ready to help, to give an advice. I hope that we will keep in touch also in future.

Then I want to thank all my family. The last three years were not easy, but you always believed in me. In spite of thousands of kilometers between us I always felt your love, care and infinite support.

This last paragraph is dedicated to a person who over the last months is near me and helps me to never give up. Marco, thank you for it.

INTRODUCTION AND STRUCTURE OF THE
DISSERTATION

1.1 Introduction

Femtocell concept has found a place in the architecture of LTE networks as a cost-effective solution designed to improve both coverage and user throughput in residential and enterprise environments (where mobile users spend most of time), as well as to offload data traffic from macrocell network. Femtocells are low-power, short-range plug-and-play cellular Base Stations (BSs) that operate in a licensed spectrum. FBSs are conceived to be installed by end consumers in ad-hoc manner, rather than being part of a planned deployment, and are connected to the service provider via the user's existing broadband Internet access (e.g. digital subscriber line or coaxial cable).

Due to the simple installation and advantages in terms of high

throughput a large diffusion of LTE femtocell devices in residential and enterprise environments is expected in the near future. This new network paradigm gives rise to some technical challenges to be addressed. Such large-scale deployment of these additional BSs may lead to a substantial increase of energy consumption of the overall cellular network. Furthermore, femtocells are conceived to share the same spectrum. That may lead to a harmful co-tier interference, which deteriorates the overall system performance. This challenge will become especially acute in dense deployments where femtocells are very likely to be overlapped. So for the success of femtocell networks the issues of energy consumption reduction and interference mitigation should be addressed conjunctly.

In this dissertation, a self-optimized coverage function for LTE femtocells embedded in a macrocell area is proposed. In our approach, each Femto Base Station (FBS) dynamically adapts its pilot power (and thus the coverage) in response to the detected on-site user activity. In a low load scenario the FBSs, whose presence is not essential for the proper operation of the network, reside in a low power Listen Mode. In this way a relevant energy saving on entire femtocell network can be achieved. In a high-load scenario, FBSs dynamically create high capacity zones under interference constraints. This permits to improve system capacity and offload more traffic from the nearby macrocell and, in the same time, to minimize co-channel interference in the femtocell tier. The proposed algorithm is fully distributed and provides highly scalable, flexible and robust control without signaling overhead, that makes it suitable for a large-scale femtocell deployment.

1.2 Structure of this Dissertation

In Chapter 2 is presented a brief overview on femtocell technology, then the main issues that arise with dense femtocell deployment are listed. In the last section of Chapter 2 is presentet a State-of-the-art overview.

In Chapter 3 we state the objectives of this dissertation, introduce the network model being considered and then present a detailed description of the proposed pilot power control algorithm.

In Chapter 4 are presented simulation results. We set optimal values of thresholds that guarantee an optimal functioning of the algorithm, evaluate scalability and robustness of our proposal, stability under changing traffic conditions. Then we evaluate an energy saving potential of our power management scheme taking into account a typical diurnal traffic pattern. Finally, we test the performance of the algorithm in a Multi-MBS environment.

In Chapter 4 we discuss the possibility of practical implementation of the algorithm.

Finally, in Appendix the formulas for calculation of decision-making parameters and system parameters are presented.

Appendix is followed by conclusion remarks, where we discuss also possible work extentions.

The list of related publication is presented as well.

MOTIVATION AND RELATED WORK

2.1 Overview on Femtocell Technology

Data traffic demand in cellular networks today is increasing at an exponential rate [1]. As the link efficiency is approaching its fundamental limits, further improvements in system spectral efficiency are only possible by increasing the node deployment density, getting the transmitter and receiver closer to each other. Studies on wireless usage show that more than 50 percent of all voice calls and more than 70 percent of data traffic originate indoors. Voice networks are engineered to tolerate low signal quality, since the required data rate for voice signals is low, on the order of 10 kb per second or less. Data networks, on the other hand, require much higher signal quality in order to provide the multi-megabit per second data rates [2]. The indoor environment is characterized by high wall penetration losses and for these reasons high data rates are difficult to achieve.

For this reason the femtocell concept has found a place in the architecture of LTE networks as a cost-effective solution designed to improve both the coverage and the user throughput in residential and enterprise environments (where mobile users spend most of time), as well as the overall system capacity by offloading data traffic from macrocells.

Femtocells, also called home base stations, are short-range low-cost and low-power base network nodes deployed by end consumers for better indoor voice and data reception. Femtocells are typically equipped with omnidirectional antennas, and their transmit power is 100 mW or less. FBSs are typically connected to the mobile core network through the consumer's own broadband connection (such as digital subscriber line (DSL) or cable modem) and therefore there is usually no backhaul transmission cost to the mobile operator.

Femtocells may be deployed on the same carrier as macrocells or on a dedicated carrier. If a dedicated carrier is used it would typically be at a higher frequency to deliver high data rates within a limited area without causing excessive interference. If femtocells share a carrier with the macrocells, it is spectrally efficient, but careful attention needs to be given to the interference that may arise between the femtocells and the macrocells.

The main benefits of femtocells can be summarized as follows.

- 1) **Improved coverage and capacity.** Due to the short scale of distances between serving cell and terminals, femtocells can achieve a high signal to interference plus noise ratio (SINR), providing an improved data reception even when there is no existing macrocell signal or poor coverage.

- 2) **Cost benefits.** For what is regarding subscribers, depending on the pricing policy mobile operators, special tariffs can be applied for calls placed under femtocell coverage. For what is regarding operators, femtocell deployments will reduce the operating and capital expenditure costs, as deployment of femtocells will reduce the need for adding macro-BS towers.
- 3) **Improved battery life.** Improved battery life for mobile devices due to reduced transmitter-receiver distance.

Femtocells generally operate in three different access modes: closed, open and hybrid. Crucially, the choice of the access mechanism influences not only the operation of the femto-tier, but also the macro-tier, and in particular cross-tier interference mitigation and handover management.

- 1) **Closed access mode.** In this mode only specified registered users can communicate with the femtocell access point (FAP). An unregistered user cannot access the femtocell even if it has the strongest link with a particular FAP. This access mode is considered to be suited for residential deployments.
- 2) **Open access mode.** The open type access control is similar to a typical macrocell. Any subscriber located within the range of the open access FAP can establish a connection with it. This access mode is considered to be used widely for enterprise deployments, in malls, cafes and other public areas. The benefit is that a large amount of traffic can be offloaded from the macrocell network to the femtocells. This is especially useful at cell edges where macrocell coverage is generally poor.

- 3) **Hybrid access mode.** Allows a limited number of unsubscribed users to gain network access alongside the existing registered users.

2.2 Technical challenges that arise with femtocell deployment

The femtocell density in urban scenarios is expected to be very high. According to the researches of “Informa Telecoms & Media”, the 9.6 million femtocells in operation today make up 56% of all base stations globally and they will continue to outnumber all other types of cells with an expected 86% of the total BS market in 2016 [3]. Due to the massive deployment of these additional BSs the wireless network energy consumption might be significantly increased.

This problem becomes especially acute if the FBSs use a static pilot power configuration based on the peak traffic load, in which they are required to transmit pilot signals continuously and to do the related processing even when they are not serving any users. This would lead to considerable energy waste for entire femtocell network under low traffic load conditions. For these reasons, energy saving techniques need to be exploited by designing efficient mechanisms to enable sleep modes in FBSs.

Another significant issue arises from the fact that femtocells are typically configured to use the same licensed frequency band as macro-cells with which they coexist. This is spectrally efficient, but can cause interference issues that become more challenging in dense FBS deployments, where femtocells are very likely to be overlapped. In such a scenario downlink transmissions from one femtocell suffer interference

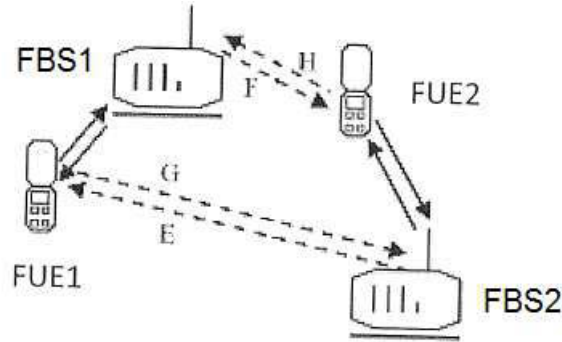


Figure 2.1: Femto-femto interference scenario.

from transmissions from another femtocell as shown in Fig. 2.1 by interference paths E and F. The increased level of interference leads to a significant performance degradation of the overall femtocell network.

For the success of femtocell networks, both the issues of energy efficiency and interference mitigation should be addressed together optimizing the potential conflicts. It is important to note also that as the FBSs are conceived to be installed by terminal consumers without network pre-planning, the approaches that address the above technical issues should be directed forward minimizing the intervention of network operator and users.

2.3 Overview on Related Works

In the literature some works have addressed co-tier interference and power consumption issues, proposing centralized or distributed pilot power control schemes and addressing the aforementioned technical challenges separately or in the aggregate.

Many studies (e.g. [4, 5, 6, 7]) deal with the method of pilot power control management that ensures a constant femtocell radius in the downlink irrespective of surrounding RF environment and deployment topology.

In the series of works [4, 5, 6] authors propose to save energy by turning into idle mode those femtocells which are not serving any active users. Idle FBS disable its pilot transmission and associated processing that represent the strongest contribution to the femtocell system power consumption.

Besides, three mechanisms of activation of idle femtocells are proposed. These mechanisms differ fundamentally in terms of the placement of activation control in the network, which can be either at the small cell, in the core network, or driven by the UE.

1) *Small cell controlled sleep mode* [4, 5, 6] Assuming the presence of sufficient underlay macrocell coverage, authors propose to equip FAPs with a low-power sniffer that permits the detection of the presence of nearby MUEs. A UE, which is served by the MBS, likely transmits with high power, hence it is easy to detect. The detection threshold is computed at a femtocell by estimating the path loss to the MBS, such that UEs located at the femtocell edge can be correctly detected. Henceforth, when an UE is detected, the FAP switches to active mode and if the UE has the right to access the femtocell, the handover process is initiated. Otherwise, the FAP reverts to the switch-off mode. Simulation results show the proposed approach can lead to high energy gain. However the algorithm is adapted to the case when just one user is present in the femtocell coverage area. In high density scenarios the aggregate energy received from different sources of interference can cause false alarm events that affect detection reli-

ability.

2) *Core network controlled sleep mode* [4, 5] In this scheme, the femtocell activity is managed by the core network that is in charge to transmit, via the backhaul, a specific wake-up control message. When a UE connects to the MBS, the core network exploits the knowledge about the UE and FAPs positions to verify if there is any UE-associated small cell in the same macrocell region. The core network driven method provides better activation control. Besides, this solution has the advantage of distinguishing between registered UEs that can be served only by open/hybrid access femtocells. But this approach implements a centralized decision that considers global knowledge on the status of the network that may be unfeasible in the next-generation femtocell deployments, where their location is random and unknown to the operator. Besides, the scheme it incurs control signaling over the backhaul to wake up small cells.

3) *UE controlled sleep mode* [4, 5] In this case the sleep mode control is placed at the user's side. A UE broadcasts the wake-up message in order to activate idle femtocells in its vicinity. This message could include identification information such that closed access femtocells wake up only for registered UEs. Idle FBSs are required to retain capability to receive the wake-up signal transmissions from the UE, and any time such signals are received, the transition to active state occurs. The UE-controlled scheme suffers mainly from two drawbacks. First, it increases UE battery consumption due to periodic broadcasts. Furthermore, it requires the specification of a robust physical/logical wireless control channel where the UE can send the wake-up message.

In [7] a clustering based power saving scheme with fixed cell radius is proposed. The algorithm divides the femtocell network into clusters

by means of femto-gateway that assigns leader and members for every cluster. The leader is responsible for detecting active calls in its cluster coverage area and for coordination of the member FBSs, which in the absence of the active user can be switched off according to leader commands.

In [8] is proposed a distributed scheme of adaptive pilot power control for FBSs which focuses on minimization of interference between residential femtocells and the outdoor macrocell.

The above mentioned power management schemes [4, 5, 6, 7, 8] have their own advantages and disadvantages. But the common fact is the absence of any coverage coordination between femtocells. This means that in dense heterogeneous deployments the coverage areas of adjacent femtocells can overlap causing a serious co-tier interference. In [9, 10, 11] adaptive power control schemes are presented which permit to overcome this issue.

In [9] is developed a distributed power control scheme for enterprise femtocell networks based on information exchange between neighboring femtocells. The algorithm periodically adjusts femtocell's pilot power to share system user load and minimize coverage holes and overlap. However, the energy saving issue is not addressed. In [10, 11] are introduced centralized approaches for dynamic power calibration which envisage a local femtocell management unit. In [10] the scheme includes UE-controlled sleep mode for FBSs in order to reduce power consumption. The FBS that receives the strongest wake-up signal level, broadcasted by UE, is chosen by Femtocell Management Unit to be waken-up. Then each active FBS adapts its transmission power as a function of UEs positions. In [11] FBSs use user activity detection in order to save energy. Active FBSs adjust their pilot power

levels in order to minimize co-tier interference following commands of Femtocell Interference Unit.

Table 2.1 synthesizes the main features of the analyzed power control management schemes. The first column indicates the bibliography reference of compared approaches. Second column (Architecture) indicates whether the type of operation of each scheme is centralized, semi-distributed, or distributed. Third column (Coverage) indicates whether each scheme considers coverage aspects such as the SINR or the receiver's sensitivity, i.e., minimum required power. Coverage analysis is crucial due to the fact that overlapping of adjacent cells leads to co-tier interference. Fourth column (Cooperation) indicates the kind of cooperation that is exploited by the FBS. A FBS can cooperate with the underlying MBS, with neighboring FBSs, or both types of coordination can be implemented. Obviously, cooperation has a direct impact on both the overhead of signaling, which is indicated in the last column (Signaling).

As it can be seen, the majority of schemes require centralized operation or consider signaling exchange between the nodes of the network. Although the centralized global knowledge-based architectures may provide better performance than distributed, the feasibility is often a concern. Such approaches require a central controller and information exchange between femtocells and the controller that may cause considerable signaling overhead. Moreover, centralized implementations may suffer a low scalability. The distributed power calibration is simple, efficient and requires minimal technician assistance, thus making it attractive for practical use.

Table 2.1: *Summary of Related Work*

| Reference | Architecture | Coverage | Cooperation | Signaling |
|--------------------------|----------------------|----------|-------------|-----------|
| [4, 5, 6], Small cell | Distributed | x | No | No |
| [4, 5], Core Network | Centralized | x | Macro | Yes |
| [4, 5], UE | Distributed | x | No | No |
| [7] | Centralized | x | Femto | Yes |
| [8] | Distributed | Yes | No | No |
| [9] | Semi- distributed | Yes | Femto | Yes |
| [10] | Centralized | Yes | Controller | Yes |
| [11] | Centralized | Yes | Controller | Yes |

PILOT POWER CONTROL APPROACH

3.1 Problem Formulation

In this dissertation is introduced a novel approach for pilot power optimization for LTE femtocell networks that addresses both energy consumption reduction and femto–femto interference issues. The objectives are following:

- 1) Improve EE of the femtocell network in a low load scenario.
- 2) Improve the overall system capacity in high load conditions and offload more traffic from the outdoor macrocell by maximizing the total coverage within the specified area where femtocells are deployed.
- 3) Reduce co–channel interference between adjacent femtocells by minimizing coverage overlaps with the view of guaranteeing a sufficient level of Signal to Interference plus Noise Ratio (SINR) to all

femtocell users (in order to provide the minimum required Quality of Service (QoS)).

- 4) Provide a robust, flexible, scalable and stable control scheme suitable for a large-scale femtocell deployment.

To fulfill the objectives, we have chosen a fully distributed measurement-based control scheme without any signaling exchange between the nodes of the network. In our approach, each FBS each FBS integrates automatic and autonomous procedures of configuration and optimization of coverage in response to the detected on-site user activity. In a low load scenario some FBSs, whose presence is not essential for the proper operation of the network, reside in a low power consumption state, that permits to achieve a relevant energy saving on entire femtocell network. In the case of a high user activity, FBSs dynamically create high capacity zones under interference constraints, adapting their pilot power configuration to the current traffic load. In addition, the stability of our algorithm was obtained considering that the femtocell size does not have significant impact on the energy consumption of the FBS [12]. So, once an active FBS has adapted its configuration to the current traffic demand, it switches to Stabilization State rather than continuously adapt its pilot power as a function of users' positions (that may result in an increased number of computational processes and handovers).

3.2 Network Model

In this dissertation a two-tier heterogeneous network comprising a single macrocell embedded with a set of FBSs is considered (Fig. 3.1).

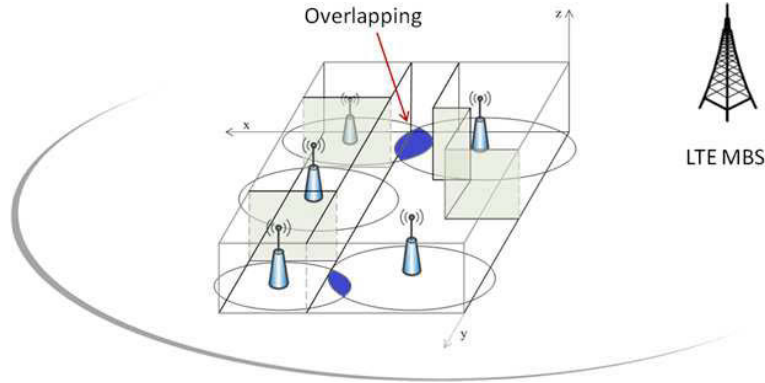


Figure 3.1: Scenario: dense femtocell deployment.

This configuration may represent residential or enterprise environments. Both FBSs and the Macro Base Station (MBS) are assumed to operate using the same OFDMA technology and to share the same licensed frequency band. We assume that the MBS ensures complete coverage, as this is the case in dense urban areas where femtocells are likely to be deployed as hotspots of large capacity for the purpose of increasing the throughput and offloading traffic from macrocells.

Femtocells are deployed without cell pre-planning and offer services to indoor UEs located in their coverage area. The MBS serves outdoor UEs and indoor UEs that are not under the coverage of active FBSs. All BSs are equipped with omni-directional antennas. For convenient analysis, some assumptions are made and are listed below.

Assumption 1. There is no intra-cell interference in the downlink.

Assumption 2. For FBSs the open access mode is adopted, i.e. FBSs behave as regular BSs and are accessible by any UE.

Assumption 3. Each UE can be served by at most one BS. Cell selection is based on a maximum downlink received power of pilot signal.

Assumption 4. FBSs operate in two modes: Listen Mode and Active Mode [6].

Based on “*Assumptions 2–3*”, the macro–femto interference is less acute than femto–femto interference. In fact in this scenario UEs which are causing or suffering from interference can be handed over freely between the macro and femtocells [13]. For example, if a macro UE is near the edge of the macrocell and is also close to a close access femtocell, then it will be transmitting at high power and may interfere with the uplink of a small cell. If the macro UE can be handed over to the small cell, the interference to the small cell would be eliminated. Similarly in the downlink, a macro UE near the macrocell edge might suffer interference from a nearby small cell, which would be eliminated if the macro UE could be handed over to the femtocell [13]. Furthermore, specific macro–femto interference mitigation approaches (e.g. [14, 15, 16]) can be additionally applied without deteriorating the performance of our power control scheme. For this reason we focus only on the problem of femto–femto interference.

3.3 Algorithm Description

In this section we present the description of the algorithm in regard to a single FBS_{*k*}, as the proposed pilot power control mechanism is measurement–based and does not require a global knowledge on the status of the network (which is peculiar to centralized solutions). Fig. 3.2 illustrates the FBS’s State Diagram and synthesizes the whole proposed power control mechanism.

Femtocells can reside in two principal operation modes: Listen

Mode and Active Mode. The FBS that resides in Listen Mode disable its pilot power and associated processing, thus it achieves a significant energy saving. In Active Mode the FBS dynamically calibrates its pilot power (and thus the coverage) as a function of local traffic demand by carrying out a two step procedure that includes Initial Power Setting and Dynamic Power Adaption. As soon as an optimal configuration is achieved, the FBS switches to Stabilization State with constant setting of the pilot power.

Operation of the proposed algorithm is based on estimation of two decision-making parameters by FBS_k :

- 1) the noise level on the uplink frequency band ($NOISE_{UL_k}$) measured by the FBS_k for detecting the presence of any active user;
- 2) the minimal value of the set which consists of wideband SINR levels ($wSINR_k$) measured by each active user connected to the FBS_k and fed back to it for detecting harmful interference.

The detailed description of the decision-making parameters is given in Appendix. By comparison of these estimated values with the corresponding thresholds ($NOISE_{TH}$ and $SINR_{TH}$ respectively) each FBS makes a decision on its pilot power calibration. In the following the detailed description of the algorithm is provided.

3.3.1 Listen Mode

In the initial state, when the local traffic demand is low or absent, the FBS without any active call resides in a low power Listen Mode with the pilot transmission and the associated processing disabled. Femtocell activity is controlled by a low-power sniffer integrated in

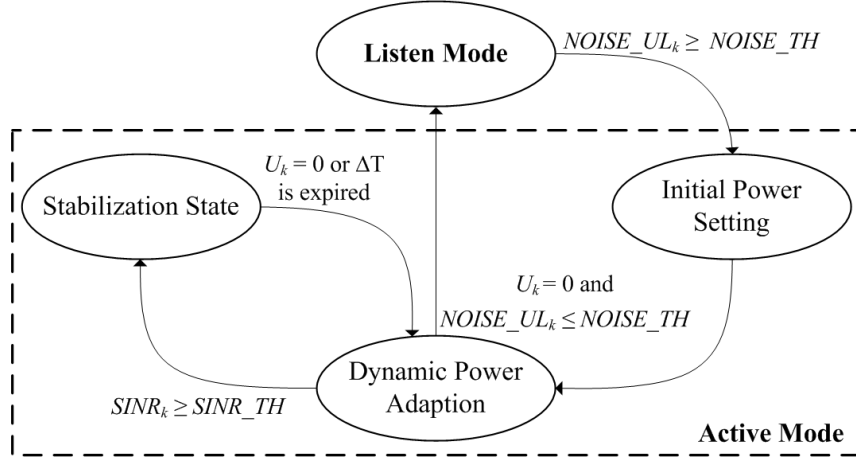


Figure 3.2: State diagram in regard to a single FBS_k.

the FBS, that continuously performs measurements of $NOISE_UL_k$. When a UE, located inside the sensing range of the sniffer, connects to the MBS, the sniffer detects a rise of the received noise power and the presence of active user can be detected. To avoid an unreasonable activation of idle femtocells we have introduced a threshold value of noise level ($NOISE_TH$), which allows to control the sensitivity of FBSs.

3.3.2 Initial Power Setting

When the sniffer detects an adequate rise in the received noise power on the uplink frequency band, that is $NOISE_UL_k > NOISE_TH$, the FBS_k switches on its pilot transmission and the associated processing, providing cell coverage with initial radius R_{ini} . For this purpose, the FBS sets the initial transmit power to such a value that a user located at the edge of the femtocell with radius R_{ini} receives, on aver-

age, the same power from the FBS and from nearby MBS. Therefore, the initial femtocell pilot power, subject to the maximum limit power of the FBS $P_{f,max}$, can be calculated in dBm as in [17]

$$P_{k,ini} = \min(P_{r,k}^{MBS} + PL(R_{ini}), P_{f,max}), \quad (3.1)$$

where $P_{r,k}^{MBS}$ is the pilot power of MBS received by FBS_k; $PL(R_{ini})$ is the estimated path loss from the femtocell to a UE at the target radius R_{ini} .

The path loss models used in the dissertation are given in Appendix.

The received power $P_{r,k}^{MBS}$ is not estimated using a path-loss model, but it is measured using the built in measurement capability of the FBS. This approach has the advantage that no information on the macrocell network is required.

Then, active UEs located within the coverage of FBS_k can detect the presence of two BSs, macro and femto, and can make a handover based on “*Assumption 3*”. Users offloaded to the femtocell have larger peak throughputs as they are close to their serving BS. In addition, those UEs who are still connected to the MBS enjoy more resources as they are shared now with a fewer number of macrocell users.

3.3.3 Dynamic Power Adaption

The Initial Power Setting procedure described above, which provides the initial cell coverage of the FBS, is optimized by Dynamic Power Adaption scheme.

Iteratively, FBS_k estimates the decision-making parameters

($NOISE_UL_k, wSINR_k$), compares them with corresponding thresholds and calibrates its pilot power accordingly until finding an optimal power configuration which accomplishes the objectives 2 and 3 of Chapter 3 Section 1. Then it switches to Stabilization State.

Below we list all the considered cases and provide some explanatory notes.

1) There are active UEs linked to the FBS_k , i.e. $U_k \neq 0$

1.a) $NOISE_UL_k \geq NOISE_TH$ & $wSINR_k \geq SINR_TH$

If both decision-making parameters exceed corresponding thresholds, it means that there are other active UEs connected to the MBS in the sensing range of the sniffer and in the same time the minimum QoS requirement of each own active UE is ensured. In this case FBS_k has to increase its cell radius, $R_k(i-1)$, of ΔR^+ aiming to provide the coverage to more UEs. Accordingly, FBS_k adapts its pilot power as follows

$$R_k(i) = R_k(i-1) + \Delta R^+; \quad (3.2)$$

$$P_k(i) = \min(P_{r,k}^{MBS} + PL(R_k(i)), P_{f,max}), \quad (3.3)$$

where ΔR^+ is the range modification step, i is the iteration number.

This case is illustrated by Fig. 3.3.

Then active UEs, located within the range of the FBS_k can detect the presence of two BSs, macro and femto, and can establish the connection based on “Assumption 3”. Users offloaded to the FBS have larger peak throughputs as they are close to their serving

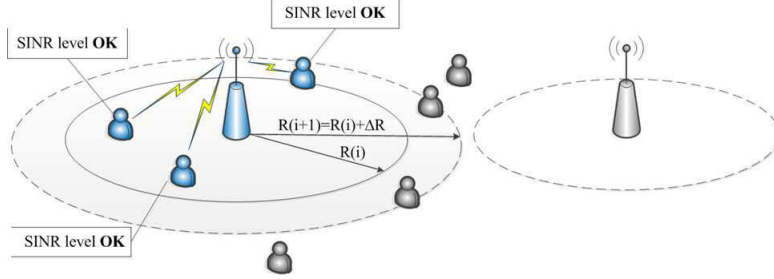


Figure 3.3: The illustration of coverage extension.

BS. In addition, those UEs who are still connected to the MBS enjoy more resources as they now share the macro cell resources with a fewer number of users.

In the next iteration the FBS will update the decision-making parameters and will verify the fulfillment of one of the conditions (1.a, 1.b, 1.c, 2.a, 2.b).

1.b) $wSINR_k \leq SINR_{TH}$

A $wSINR_k$ value below its acceptable level means that the minimum QoS requirement is not satisfied for at least one currently connected user. This user is likely to be located in the overlap area between adjacent femtocells. So FBS_k decreases its cell radius of ΔR^- by setting its pilot power in the following way:

$$R_k(i) = R_k(i-1) - \Delta R^-; \quad (3.4)$$

$$P_k(i) = \max(P_{r,k}^{MBS} + PL(R_k(i)), P_{f,min}), \quad (3.5)$$

where $P_{f,min}$ is a minimum transmit power of the FBS.

This case is illustrated by Fig. 3.4.

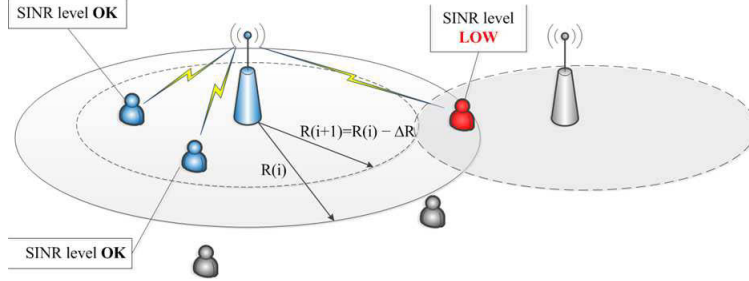


Figure 3.4: The illustration of coverage reduction.

As a result of coverage reduction, those users who were suffering from the interference appear to be out of coverage of FBS_k and they establish a new connection based on “Assumption 3”.

In the next iteration the FBS updates $wSINR_k$ value and verifies the fulfillment only of condition (1.b). So FBS_k continually decreases its pilot power until $wSINR_k \geq SINR_{TH}$, then its pilot power remains constant irrespectively to $NOISE_{UL_k}$ value. This decision allows to eliminate continuous variations of the coverage area in order to avoid an excessive number of handover events and to achieve the Stabilization State.

1.c) $NOISE_{UL_k} < NOISE_{TH}$ & $wSINR_k \geq SINR_{TH}$

FBS has achieved an optimal coverage and it switches to Stabilization State and its pilot power remains constant.

2) No active UE linked to the FBS_k , i.e. $U_k = 0$

If there are not currently connected active UEs, FBS_k adapts its coverage according only to $NOISE_{UL_k}$ value.

2.a) $NOISE_{UL_k} \geq NOISE_{TH}$

It means that there are active macro UEs located in the sensing range of the sniffer.

If $P_k \leq P_{f,max}$, the FBS increases its pilot power according to (3.4). Due to the coverage extension some active macrocell users can handover into the femtocell based on “*Assumption 3*”. In the next iteration the FBS updates the decision-making parameters and verifies the fulfillment of one of the conditions (1.a, 1.b, 1.c, 2.a, 2.b), adapting its pilot power setting accordingly.

If FBS_k has achieved the maximum value of its pilot power ($P_k = P_{f,max}$), while macro UEs remain unattainable ($U_k = 0$), FBS_k turns off its pilot power and associated processing and rests in Listen Mode for ΔT time interval. So, FBS_k will reside in an energy saving state, rather than being active measuring a high $NOISE_UL_k$ level due to transmissions of unattainable UEs.

2.b) $NOISE_UL_k < NOISE_TH$

The FBS turns off its pilot transmission and associated signaling and returns to the Listen Mode processing.

The Dynamic Power Adaption procedure is summarized in Fig. 3.5.

3.3.4 Stabilization State

The FBS achieves Stabilization State when its pilot power (and thus the coverage) is optimized based on the on-site traffic demand and in the same time an acceptable SINR level is guaranteed to each of its currently connected user. From Stabilization State, FBS_k switches to Dynamic Power Adaption procedure in order to detect changes of

the local radio environment and, if required, updates its pilot power setting. The transition to Dynamic Power Adaption is carried out: periodically with time intervals ΔT if there are active UEs currently connected to FBS_k or immediately when no UE is connected to FBS_k , i.e. $U_k = 0$ is verified.

Definition: U_k is a number of active users linked to the FBS_k .

Initialize: Stabilization State \leftarrow FALSE.

```

1. while Stabilization State  $\leftarrow$  FALSE
2.   Update  $NOISE_{UL_k}$  and  $U_k$ 
3.   if  $U_k \geq 1$ 
4.     Update  $wSINR_k$ 
5.     if  $NOISE_{UL_k} \geq NOISE\_TH$  &  $wSINR_k \geq SINR\_TH$ 
6.       Increase pilot power:
7.        $R_k \leftarrow R_k + \Delta R \Rightarrow P_k \leftarrow \min(P_{r,k}^{MBS} - PL(R_k), P_{f,max})$ .
8.     end if
9.     if  $wSINR_k < SINR\_TH$ 
10.      while  $wSINR_k \leq SINR\_TH$ 
11.        Decrease pilot power:
12.         $R_k \leftarrow R_k - \Delta R \Rightarrow P_k \leftarrow \max(P_{r,k}^{MBS} - PL(R_k), P_{f,min})$ .
13.        Update  $wSINR_k$ 
14.      end while
15.      No pilot power modification:  $R_k \leftarrow R_k \Rightarrow P_k \leftarrow P_k$ .
16.      Stabilization State  $\leftarrow$  TRUE.
17.    end if
18.    if  $NOISE_{UL_k} < NOISE\_TH$  &  $wSINR_k \geq SINR\_TH$ 
19.      No pilot power modification:  $R_k \leftarrow R_k \Rightarrow P_k \leftarrow P_k$ .
20.      Stabilization State  $\leftarrow$  TRUE.
21.    end if
22.  else
23.    if  $NOISE_{UL_k} \geq NOISE\_TH$ 
24.      if  $P_k < P_{f,max}$ 
25.        Increase pilot power:
26.         $R_k \leftarrow R_k + \Delta R \Rightarrow P_k \leftarrow \min(P_{r,k}^{MBS} - PL(R_k), P_{f,max})$ .
27.      else
28.        Turn off pilot transmission:  $R_k \leftarrow 0 \Rightarrow P_k \leftarrow 0$ .
29.        Return to Listen Mode processing after  $\Delta T$ , break.
30.      end
31.    else
32.      Turn off pilot transmission:  $R_k \leftarrow 0 \Rightarrow P_k \leftarrow 0$ .
33.      Return to Listen Mode processing, break.
34.    end if
35.  end if

```

Figure 3.5: Dynamic Power Adaption.

PERFORMANCE EVALUATION

In this chapter we verify the performance of the proposed scheme by simulations in MATLAB. Firstly we set optimal values of thresholds that guarantee an optimal functioning of the algorithm. After that we show scalability and robustness of our proposal changing the femtocell deployment topology and considering different distances of the group of FBSs from the MBS. Then the stability under changing traffic conditions is evaluated. Then we evaluate an energy saving potential of our power management scheme taking into account a typical diurnal traffic pattern. Finally, we test the performance of the algorithm in a Multi-MBS environment.

4.1 Simulation assumptions and performance metrics

The system parameters setting used in the simulations can be found in Appendix. More specifically, some assumptions and simplifications were made: all UEs have “Power class 3” ($P_{max} = 23$ dBm), defined by the standard; all FBSs have the same maximum transmission power $P_{f,max}$; P_0 and α values are equal for all FBSs; UEs belong to two different traffic classes: Low-Rate users and High-Rate users with different number of allocated Physical Resource Blocks (PRBs).

As regards the traffic load, in our simulations we consider N_u active UEs (50% are Low-Rate users and 50% are High-Rate users) uniformly distributed, or, alternatively, concentrated in the macrocell area.

Furthermore, we have defined the following metrics.

- 1) Overlapping factor of femtocells (Θ).

$$\Theta = \frac{\sum_{i=1}^N \sum_{j=i+1}^N \Theta_{i,j}}{\sum_{i=1}^N A_i - \sum_{i=1}^N \sum_{j=i+1}^N \Theta_{i,j}}, \quad (4.1)$$

where N is the total number of FBSs; A_i is the area covered by femtocell i ; $\Theta_{i,j}$ is the overlap area between femtocell i and femtocell j .

- 2) Percentage of users present in the macrocell area served by all FBSs (Φ).

$$\Phi = \frac{\sum_{i=1}^N U_i}{N_u} \cdot 100, \quad (4.2)$$

where U_i is a number of users served by FBS $_i$; N_u is a total number of active users present in the macrocell area.

In the following for assessing the performance of our coverage function we compare it to the static pre-planned configurations, where the pilot power of each FBS is fixed and is ideally set to provide the maximum coverage with minimal femto-femto interference by excluding overlap between adjacent femtocells (see, for example, Fig. 4.1).

4.2 Determination of thresholds

As the proposed algorithm requires to set optimal values of the thresholds $SINR_{TH}$ and $NOISE_{TH}$, we have firstly set $SINR_{TH} = -4$ dB and then determined an optimal $NOISE_{TH}$ value by carrying out a series of simulations. Notice that according to [18] the above value chosen for $SINR_{TH}$ is defined by LTE specifications like a

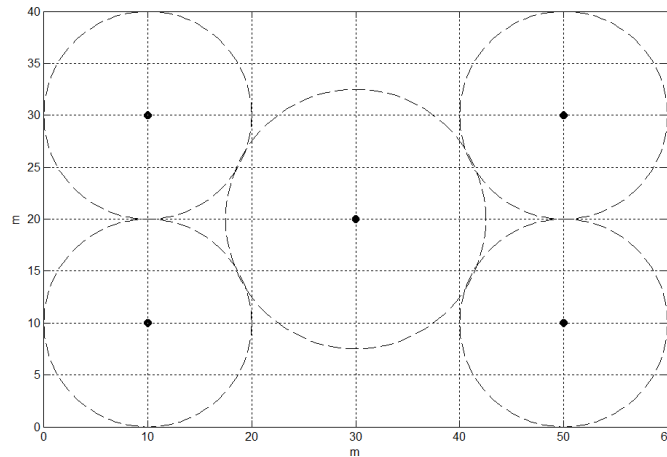


Figure 4.1: Static configuration.

minimum SINR required to guarantee satisfactory QoS.

The scenario used to simulate and evaluate an optimal *NOISE_TH* value represents an enterprise environment with 5 FBS (see Fig. 4.1) localized so as to cover most part of an area ($60 \times 40 \text{ m}^2$). We also assume that this area is covered by a MBS located at a distance of about 300 meters.

Fig. 4.2 and Fig. 4.3 show diagrams of Θ and Φ , respectively, for *NOISE_TH* varying from -60 to -50 dBm (with the step of 10 dBm). The results are averaged over 50 independent simulation runs. For the static configuration $\Theta = 0$ for different traffic load scenarios, this is because the pilot power of each FBS is constant and it is configured to avoid overlap areas between adjacent femtocells. The value of Φ , instead, is maintained around 73%. So, even such “ideal” configuration cannot guarantee the coverage to all active UEs present in the considered macrocell area. By comparative analysis of the simulation results (see Fig. 4.2 and Fig. 4.3), it can be estimated that a good trade-off between Θ and Φ is achieved with *NOISE_TH* set to -53 dBm. In fact, this threshold value provides $\Theta \leq 5\%$ and Φ is about 80% in a high load scenario.

Finally, the thresholds are set to: *SINR_TH* = -4 dB; *NOISE_TH* = -53 dBm and are used in all the following simulations. With this values of thresholds in Fig. 4.4 is shown an example of the operation of our algorithm: each FBS dynamically adapts its pilot power (fine line) according to the traffic demand until Stabilization State (bold line). Here and in all following simulation results the users present in the macrocell area are indicated by dots.

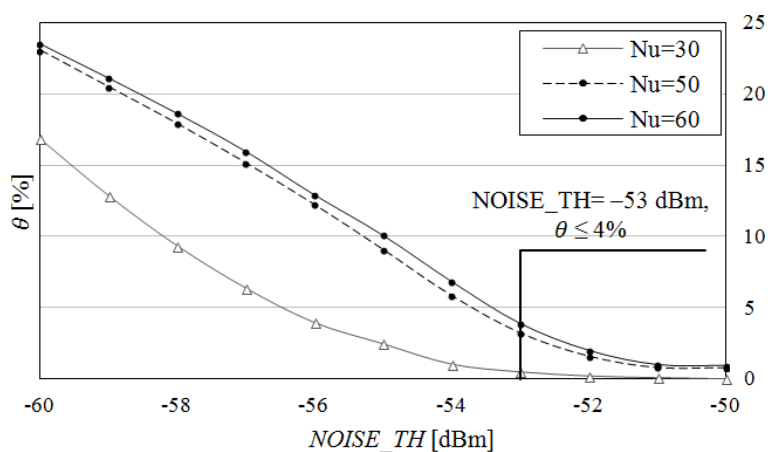


Figure 4.2: Overlapping factor of femtocells (θ) vs. $NOISE_TH$.

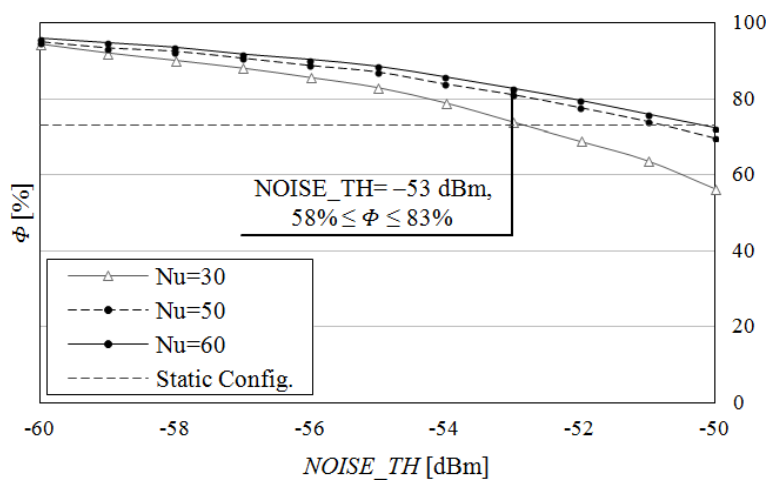


Figure 4.3: Percentage of users served by FBSs (Φ) vs. $NOISE_TH$.

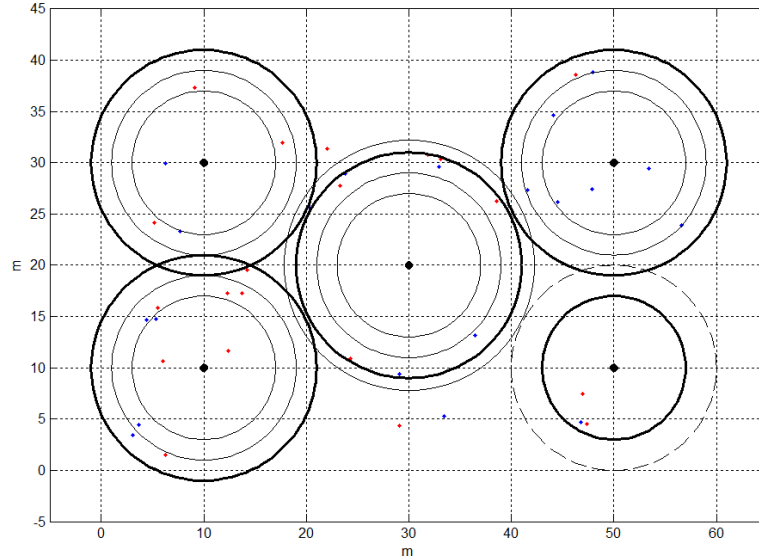


Figure 4.4: Example of the operation of proposed algorithm.

4.3 Evaluation of scalability and robustness

To evaluate the scalability and robustness of our proposal, we have carried out a series of simulations varying the network topology:

Topology 1. 5 FBS localized so as to cover most part of an area ($60 \times 40 \text{ m}^2$) (see Fig. 4.1);

Topology 2. 3 FBS localized so as to cover most part of an area ($60 \times 40 \text{ m}^2$) (see Fig. 4.5);

Topology 3. 20 FBS randomly distributed in an area ($100 \times 100 \text{ m}^2$) (see Fig. 4.6).

For all topologies, the MBS is assumed to be located at the distance of about 300 meters.

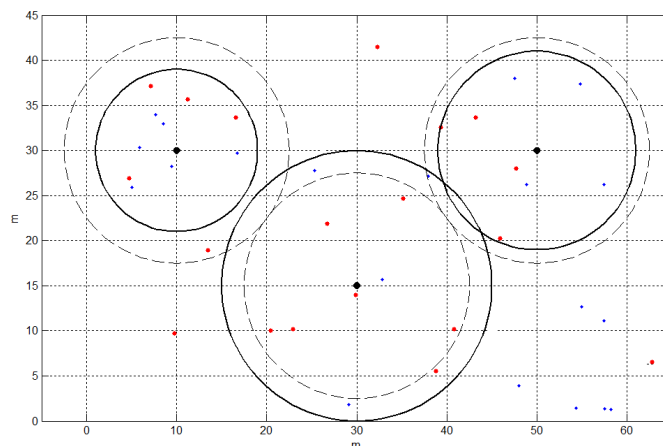


Figure 4.5: Static configuration (dotted line) and final configuration for the proposed algorithm (solid line) for Topology 3, $N_u = 70$.

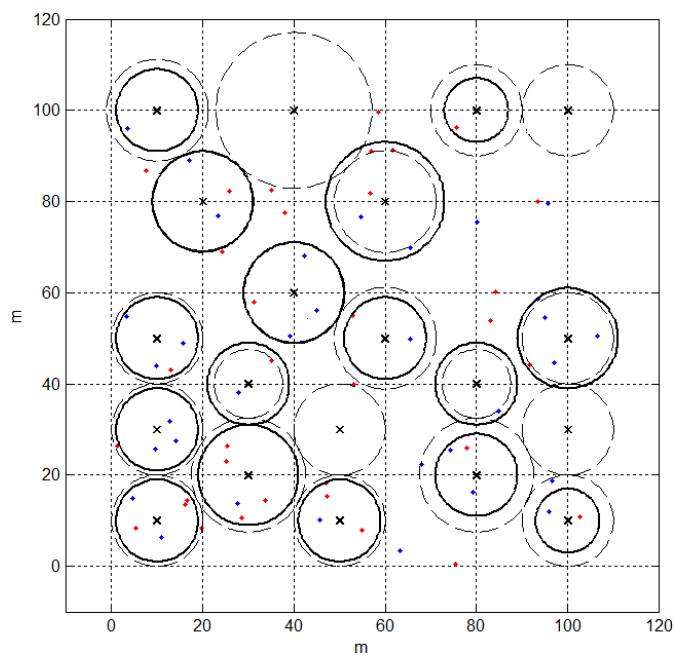


Figure 4.6: Static configuration (dotted line) and final configuration for the proposed algorithm (solid line) for Topology 3, $N_u = 70$.

In Fig. 4.7 and Fig. 4.8 are shown Φ and Θ for each topology at various UE's densities per unit area ($\rho = \text{active users/m}^2$). When the system is in low traffic conditions ($\rho \leq 0.01$), our algorithm provides lower Φ values compared to the static configuration, as in this case our power control scheme places some FBSs in Listen Mode (for instance, three FBSs reside in Listen Mode in Fig. 4.9), thus allowing to achieve a relevant energy saving on entire femtocell network. However, in this scenario the MBS can alone handle the traffic while offering to users satisfactory throughput. When the traffic load increases ($\rho > 0.01$) the proposed algorithm, thanks to its adaptive nature, allows to obtain higher Φ values compared to the static configuration (see Fig. 4.7), while maintaining an acceptable level of Θ (see Fig. 4.8). More precisely, in Fig. 4.10 is shown an example of how the algorithm is able to provide the coverage to those users (indicated by triangles) who could not be covered by the static configuration, while guaranteeing the sufficient SINR level to all connected users (minimal overlap). So, in a high load scenario our algorithm allows to offload more traffic from the MBS and therefore to increase the overall system capacity. In addition, EE of the overall cellular network also enhances, as MBS's power consumption is strongly related to its traffic load [12]. Let's note that numerical values vary depending on the specific arrangement of FBSs, but, regardless the network topology being considered, implementation of the proposed algorithm allows to offload up to 13% active users from the MBS. This confirms scalability of proposed power control scheme.

Lastly, for each topology, we have considered various distances of the FBSs from the MBS (300 m, 1 km, 5 km, 20 km and 30 km) (Fig. 4.11, Fig. 4.12, Fig. 4.13 respectively). The simulation results

differ slightly from those previous confirming flexibility and robustness of our self-coverage function.

Finally, the scalability, dynamic adaptability, and flexibility of the proposed algorithm guarantee a natural robustness to any faults or shutdown of one or more FBSs.

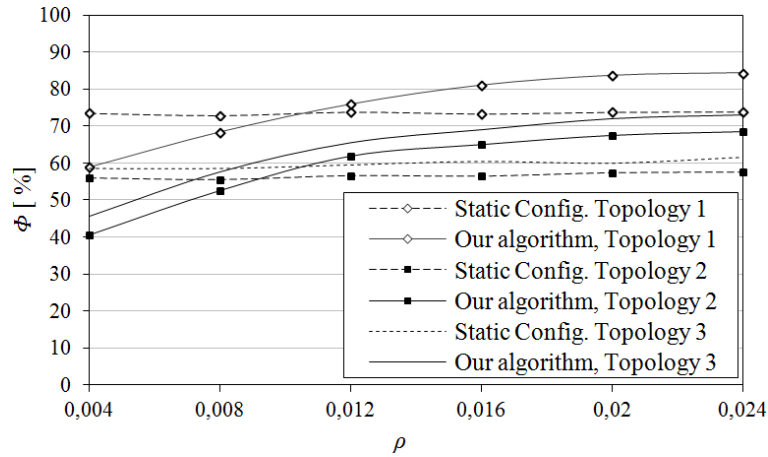


Figure 4.7: Percentage of users served by FBSs (Φ) vs. UE's density ρ .

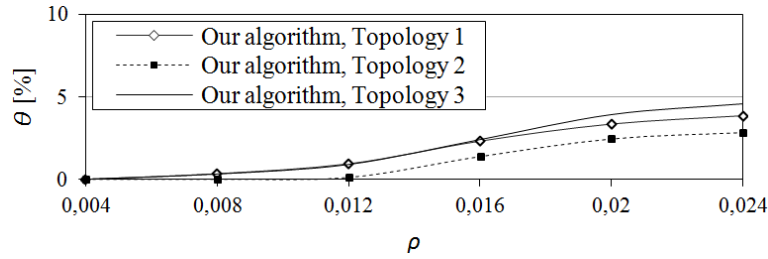


Figure 4.8: Overlapping factor of femtocell (Θ) vs. UE's density ρ .

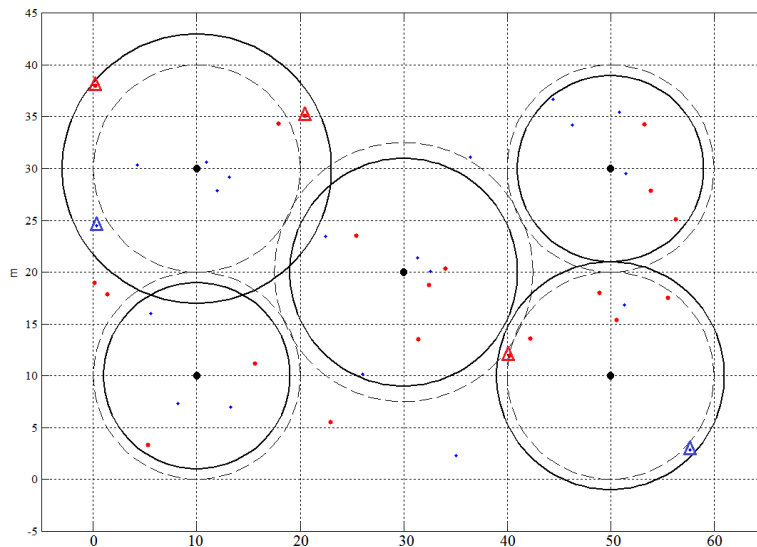


Figure 4.9: Static coverage (dotted line) and final configuration for the proposed algorithm (solid line), $N_u = 20$.

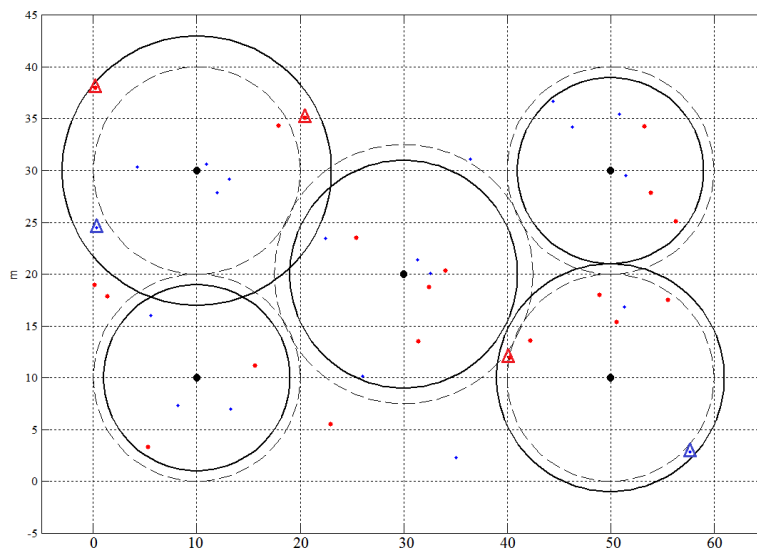


Figure 4.10: Static coverage (dotted line) and final configuration for the proposed algorithm (solid line), $N_u = 40$.

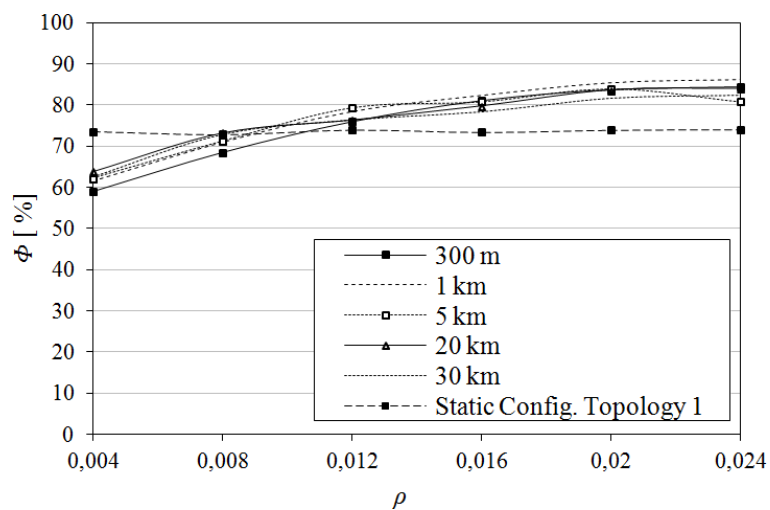


Figure 4.11: Percentage of users served by FBSs (Φ) vs. UE's density ρ for Topology 1.

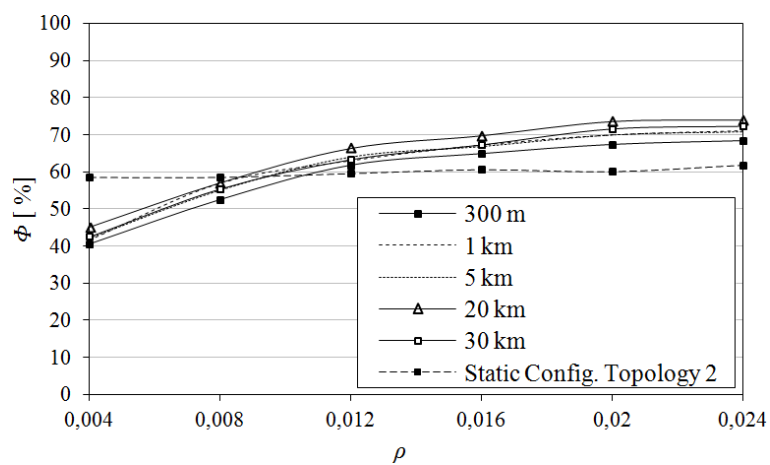


Figure 4.12: Percentage of users served by FBSs (Φ) vs. UE's density ρ for Topology 2.

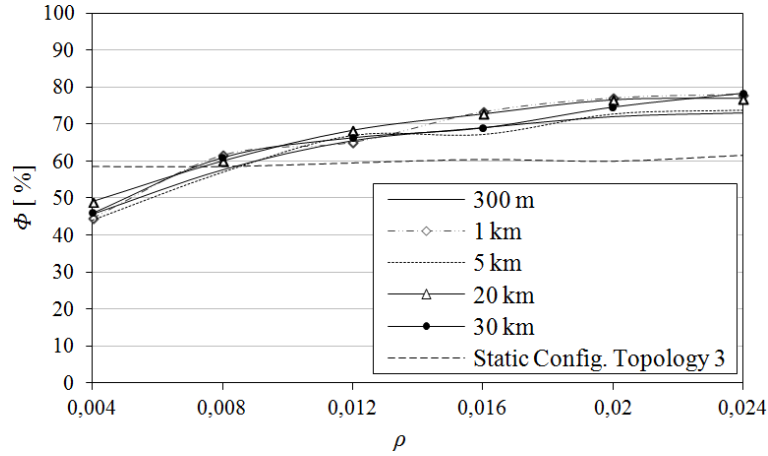


Figure 4.13: Φ vs. ρ at various distance of the group of FBSs from the MBS for Topology 3.

4.4 Evaluation of Stability

The performance of our algorithm, in terms of stability and responsiveness of the control, depends on the ΔT value, that is the time interval in which a FBS resides in Stabilization State before switching to Dynamic Power Adaption procedure.

We expect that with shorter ΔT duration the system is more responsive to the changes of traffic conditions due to the frequent pilot power adaptations. But this could result in a significant increase in the number of handover events. To determine the appropriate ΔT value, we have considered a new scenario in which the traffic load is variable in time. More specifically, the simulations have been carried out under the following assumptions:

- 1) UEs are uniformly distributed in the considered macrocell area.
The total number of UEs varies during the observation period of

16 hours (6:00 to 22:00) as shown in Fig. 4.14.

- 2) The mobility of UEs is neglected, but each UE can reside in on/off state following the Poisson Distribution process of the call arrival time. The interarrival time and the call holding time are exponentially distributed with means $\lambda = 4$ [min] and $\mu = 3$ [min] respectively.

We provide simulation results only for *Topology 1*, as due to scalability of our power control scheme analogous results can be obtained also with others.

Fig. 4.15 shows the average percentage of users covered by all FBSs during the whole observation period for several ΔT values. We observe that for $\Delta T \leq 16.5$ [min] our algorithm responds more efficiently to the traffic fluctuations and, consequently, provides higher Φ values compared to the static configuration (dotted line). However, such ΔT values lead to a substantially increased number of handovers (see Fig. 4.16) due to the frequent pilot power calibration events in attempt to continuously improve the coverage. Protracted ΔT duration delays the response of FBSs to the changes of the traffic demand and, as a consequence, adversely affects the performance of our algorithm in terms of Φ (see Fig. 4.15 for $\Delta T > 16.5$ [min]). Nevertheless, in this case the number of handovers is significantly reduced (see Fig. 4.16).

Let's also note that the total duration of Listen Mode intervals is not sensitive to ΔT values, as the FBS switches to Listen Mode if no UE is connected to it independently if ΔT is expired or not.

So, by comparative analysis of simulation results shown in Fig. 4.15-4.16 we have determined $\Delta T = 13$ [min] as an optimal value, that permits to achieve a good trade-off between the number of han-

dozer events and Φ . The next the analysis is made with $\Delta T = 13$ [min].

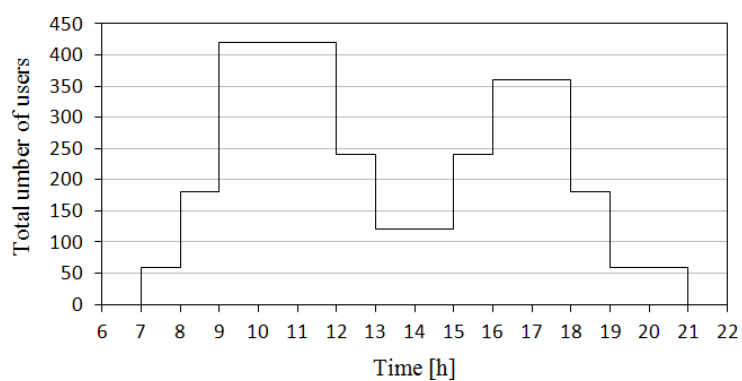


Figure 4.14: User distribution pattern.

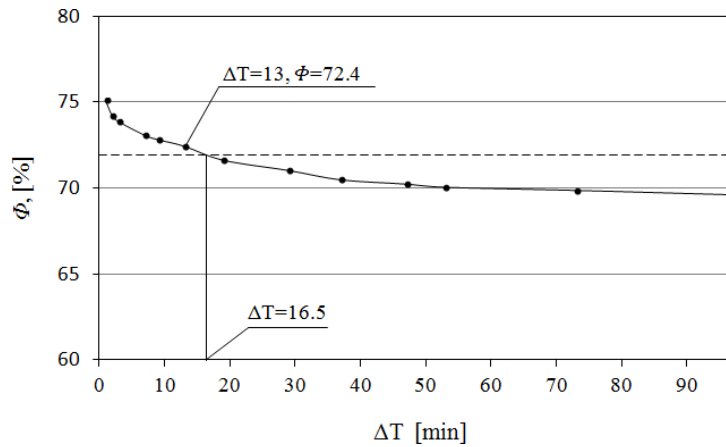


Figure 4.15: Φ vs. ΔT intervals.

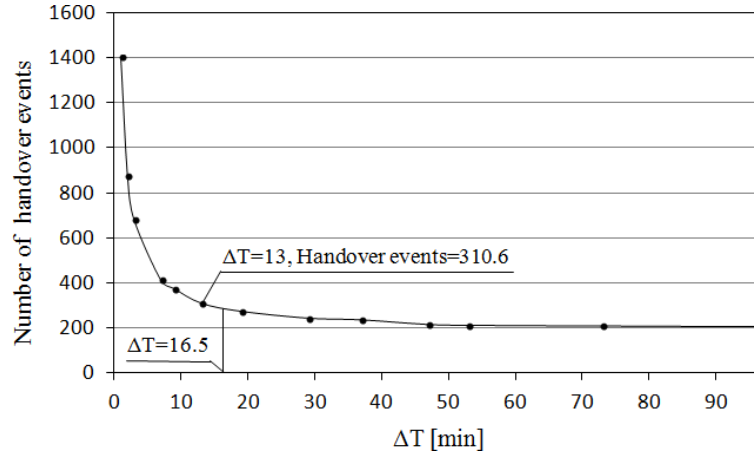


Figure 4.16: The total number of handover events vs. ΔT intervals.

4.5 Evaluation of Energy Efficiency

In the following we provide a power consumption analysis for FBS which operates in Active Mode and Listen Mode. According to [12] the power consumption is load dependent for MBSs, while there is a negligible load dependency for FBSs, so we assume static power consumption across all traffic load for FBSs and we use a static component-based power consumption evaluation model introduced in [19]. This power model is built around the split of a BS into a number of components and sub-components, as shown in Fig. 4.17.

A FBS consists of two transceivers (TRXs). A TRX comprises an Antenna Interface (AI), a Power Amplifier (PA), a Radio Frequency (RF) small-signal transceiver section, a digital baseband (BB) interface including a receiver and transmitter section, a DC-DC power supply, an active cooling system and an AC-DC unit (Main Supply) for connection to electrical power grid.

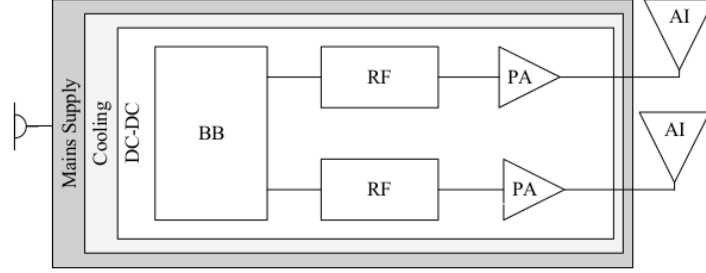


Figure 4.17: Overview of base station components included in the power model.

So, the power consumption of the FBS that resides in Active Mode can be calculated as follows

$$P_{ACT} = N_{TRX} \cdot \frac{P_{PA} + P_{RX} + P_{TX} + P_{BB} + P_{Sniff.}}{(1 - \sigma_{DC})(1 - \sigma_{MS})(1 - \sigma_{Cool.})}. \quad (4.3)$$

Table 4.1 summarizes the state of the art power consumption of LTE femtocells as of 2012. Applying the data reported in Table 4.1 to equation (4.3), we obtain $P_{ACT} = 7$ [W].

Table 4.1: LTE femtocell transceiver power consumption

| PA, [W] | TX, [W] | RX, [W] | BB, [W] | DC-DC, σ_{DC} | Cooling, $\sigma_{Cool.}$ | AC-DC, σ_{MS} | N_{TRX} |
|------------|------------|------------|------------|-------------------------|------------------------------|-------------------------|-----------|
| 1.0 | 0.2 | 0.2 | 1.2 | 0.08 | 0.0 | 0.1 | 2 |

By switching to Listen Mode, the FBS switches off the PA, RF transmitter and RF receiver. However, the sniffer ($P_{Sniff.} = 0.3$ W [6]) is switched on to perform received power measurements on the uplink frequency band. So, the power consumption of the FBS that resides

in Listen Mode results

$$P_{LM} = N_{TRX} \cdot \frac{P_{BB} + P_{Sniff.}}{(1 - \sigma_{DC})(1 - \sigma_{MS})(1 - \sigma_{Cool.})} = 3.62 \text{ [W]}. \quad (4.4)$$

As can be estimated, the addition of Listen Mode to the normal femtocell operation results in a power saving of 48.29% for each idle femtocell.

The total amount of energy consumed by FBS_k is given in the following equation:

$$E_{FBS}^k = P_{ACT,k} \cdot t_{ACT,k} + P_{LM,k} \cdot t_{LM,k}, \quad (4.5)$$

where $P_{ACT,k}$ and $P_{LM,k}$ represent the power consumption of FBS_k when it resides in Active or in Listen Mode, respectively; $t_{ACT,k}$ and $t_{LM,k}$ represent the time period (expressed in hours) in which the FBS_k is in Active Mode and in Listen Mode, respectively.

So, the total amount of energy consumed by entire femtocell network can be calculated as:

$$E_{FN} = \sum_{k=1}^N E_{FBS}^k. \quad (4.6)$$

To evaluate the energy saving potential of our algorithm in a realistic scenario we have taken into account a traffic profile that emulates the spatial and temporal variations during a working day in an enterprise scenario. More specifically, we consider *Topology 3* (Fig. 4.18) provisioned of a Dining and Lounge Area, where the number of users increases substantially during the lunch break (from 13:00 to 15:00) (as shown in Fig. 4.19).

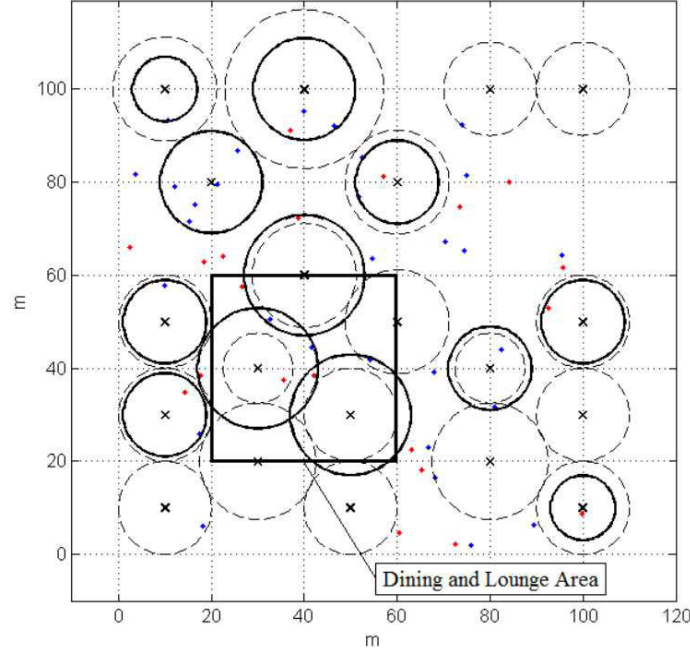


Figure 4.18: Static configuration (dotted line) and final coverage for our algorithm (solid line)–Topology 3, $\rho = 0.006$

After a series of simulations, in Fig. 4.20 we report the number of active femtocells, averaged over each hour. Besides, in Fig. 4.21 the average number of active users connected to FBSs with our algorithm and those with the static configuration are presented. Finally, in Fig. 4.22 we report the energy saving gain obtained for each hour and calculated as follows

$$E_{GAIN} = \frac{E_{FN,Static} - E_{FN,OurApproach}}{E_{FN,Static}}, \quad (4.7)$$

where $E_{FN,Static}$ and $E_{FN,OurApproach}$ are calculated according to (4.6)

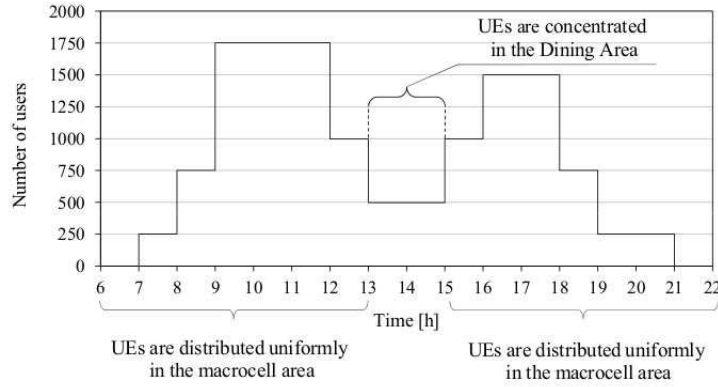


Figure 4.19: User distribution pattern.

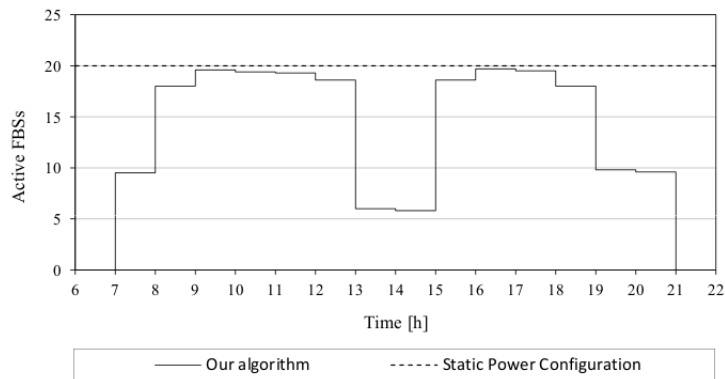


Figure 4.20: Medium number of active femtocells vs. time.

and represent the total amount of energy consumed by the whole femtocell network with the static configuration and with implementation of our algorithm, respectively.

By comparing the above results, in low load conditions numerous FBSs reside in Listen Mode, that permits to achieve a significant en-

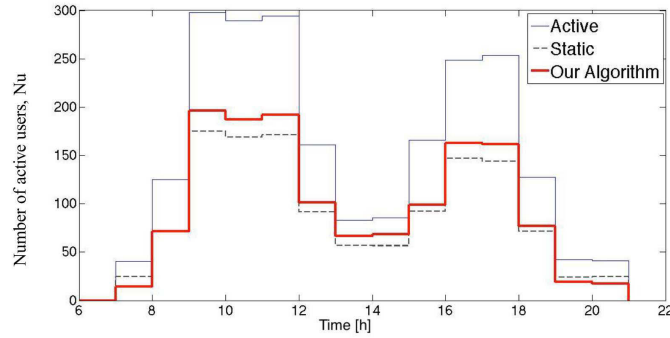


Figure 4.21: Percentage of users served by FBSs (ϕ) vs. Time of day.

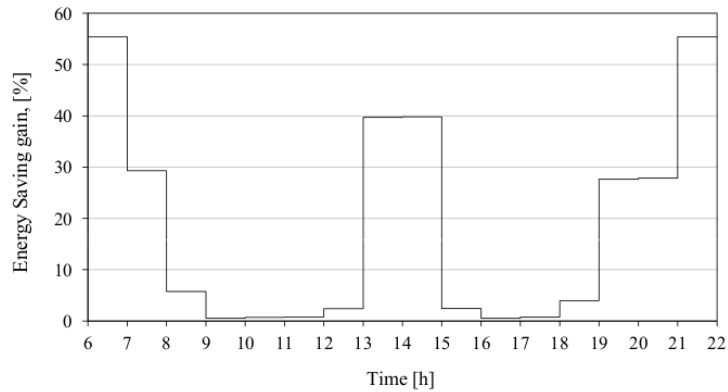


Figure 4.22: Energy Saving gain vs. Time of day.

ergy gain (see Fig. 4.22) and in the same time does not affect seriously the user coverage. In fact, as shown in Fig. 4.21, the coverage provided by our power control scheme is only marginally lower than those static. Nevertheless, in these conditions the MBS alone can provide satisfactory performance to its connected users. In high load conditions, most of FBSs are active and our control scheme provides better

coverage compared to the static configuration (Fig. 4.21) and, consequently, more traffic is offloaded from the MBS (just when it is the most necessary).

Applying (4.7) to the whole observation period, we have quantified the total amount of energy consumed by entire femtocell network during a working day: $E_{FN,Static} = 2240.00$ [Wh] and $E_{FN,Our Approach} = 1871.84$ [Wh]. It can be estimated that implementation of our algorithm in this case study results in an overall energy saving gain of 16.44%. It is important to emphasize that the total power saving of the femtocell network is relevant considering the expected large-scale deployment of FBSs in urban scenarios.

4.6 Multi-MBS environment

In this section we discuss the applicability of proposed pilot power control scheme in a multi-MBS environment. To evaluate the performance of our algorithm in such a scenario, we estimate the impact of the presence of neighboring MBS on estimation of the decision-making parameters ($NOISE_{UL}$ and $wSINR$).

We have considered two adjacent MBSs: MBS_i and MBS_j , which belong to the same operator and have equal maximal transmit powers P_t^{MBS} (see the Table with system parameters setting in Appendix). The MBSs are located at the distance $L_{i,j} = 3$ [km] from each other. In the coverage area of MBS_i is embedded a FBS at the distance d_i from it (see Fig. 4.23).

4.6.1 *NOISE_UL* estimation in multi-MBS scenario

For distances $d_i < L_{i,j}/2$, the presence of neighboring macrocell does not affect the performance of our algorithm, since in such a scenario UEs would be connected to the MBS_{*i*} (based on “*Assumption 3*”). The presence of adjacent MBS_{*j*} would have an impact only at the cell edge, where UEs, located in the vicinity of the FBS, could be connected to different MBSs. *NOISE_UL* parameter estimation will not be affected even in this scenario, as it represents the total noise power in the uplink frequency band irrespectively to the choice of serving cell by UEs. This is because our pilot power control scheme is self-organizing and without any intercell signaling exchange. What may happen is that the idle FBS would measure an elevated *NOISE_UL* level and would switch to Active State not only due to the presence of UEs connected to MBS_{*i*}, but also due to transmissions of those connected to MBS_{*j*}. It will not cause any negative effect on the operation of our algorithm. On the contrary, at the edges of the cell, where users experience the worst conditions in terms of channel quality and bandwidth, femtocells will be switched on providing better performance to users.

4.6.2 *wSINR* estimation in multi-MBS scenario

To evaluate the impact of adjacent MBS on the *wSINR* estimated by femtocell users, we have assessed downlink interference variations with different distances of the FBS from MBS_{*i*} and from MBS_{*j*}. We have considered a worst-case scenario, where a FBS, located in the coverage

area of MBS_i , is moving radially with respect to both MBSs ($d_i=(100, L_{i,j}/2)$ [m], see Fig. 4.23). In this way, when the distance increases from one MBS by Δd , the distance from the other MBS decreased by equal value (Δd) and the interfering effect becomes more sensitive.

The simulation results show that when the FBS is close to MBS_i , the interference power that would receive a femtocell UE from MBS_j (I_{MBS_j}) is negligible compared to those from MBS_i (I_{MBS_i}). The interference power received from both MBSs reaches its maximal value at the cell edge, where the aggregate MBSs' interference doubles ($I_{MBS_j} + I_{MBS_i}$). However, the aggregate interference power received from both MBS_i and MBS_j at the cell edge is lower than the interference that users would experience when they are connected to a FBS located next to one of MBSs.

The provided analysis show that the performance of our pilot power control scheme of are not affected by the presence of neighboring MBSs in a multi-MBS environment.

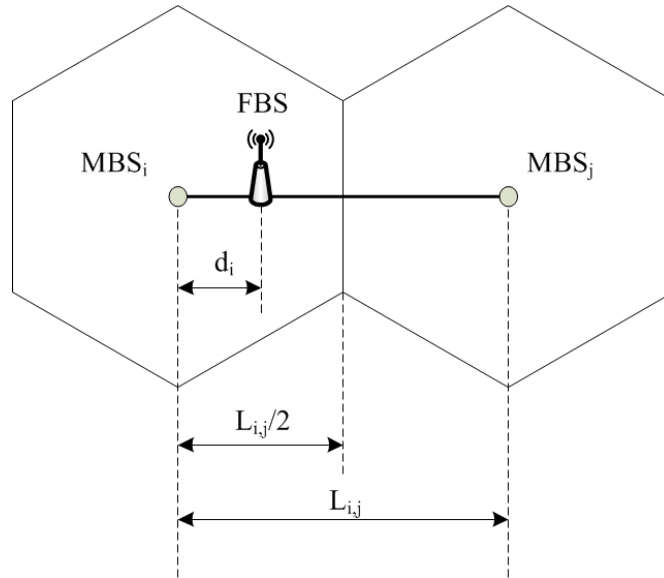


Figure 4.23: Multi-MBS simulation scenario.

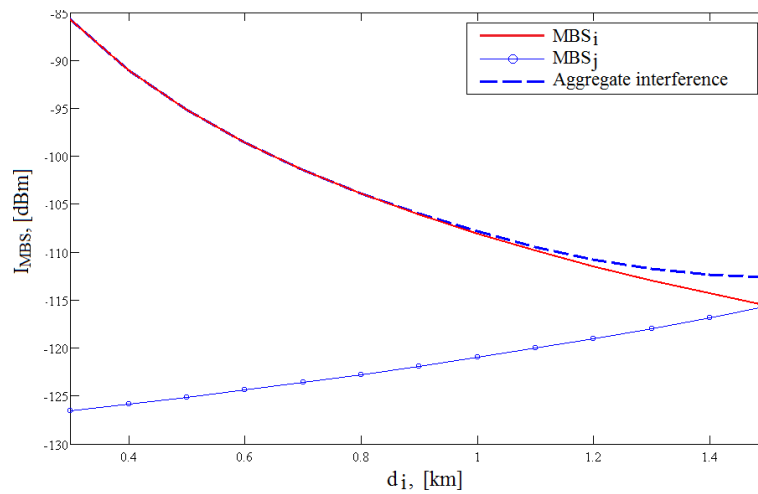


Figure 4.24: Interference power received from MBS_i and MBS_j vs. distance from MBS_i.

IMPLEMENTATION ISSUES

In this chapter we propose some methods for practical implementation of proposed pilot power control mechanism. As our approach is based on two decision-making parameters: $NOISE_{UL_k}$ (measured by each FBS) and $wSINR_k$ (measured by each active femtocell user), the practical implementation issues are related to estimation of these parameters.

5.1 Network Listen Mode

For the practical implementation of the sniffer for measurement of the uplink noise level a femtocell would require only an additional uplink receiver that can perform correlation between signals. This receiver is analogous (operates in the same frequency band) to those used to receive uplink traffic. The duplication of the uplink receiver would bring just an insignificant extra cost.

Either way, the sniffing capability is often already integrated into femtocells. The key vendors produce LTE FBSs equipped with the Network Listen Module (NLM) which facilitates the plug-and-play deployment of femtocells (see Table 5.1). It permits to the femtocell to make measurements of surrounding macrocells and femtocells in order to optimize its configuration settings. NLM can be used in our approach to perform measurements of noise level on the uplink frequency band and as the module is already integrated into femtocell such a solution incurs no extra cost.

Table 5.1: *Femtocell market status*

| Vendor | Product name |
|-------------------|-----------------------------------------------------------------------------------------------------------------|
| ip.access Limited | nanoLTE Access Points family (femtocells for enterprise and public access): nanoLTE E-40, nanoLTE+ E-100 |
| Cisco Systems | Cisco Aironet 3600 Series and Cisco Universal Small Cell 5310 |
| Alcatel-Lucent | 9760 Small Cell product family |
| Fujitsu | BroadOne LS100 Series LTE femtocell (residential), BroadOne LS200 Series LTE femtocell (semi-public/enterprise) |

5.2 SINR

The SINR calculation is not defined in the 3GPP specifications but it is defined by femtocell vendors, as this parameter is used a lot by operators and the LTE industry in general. As consequence, the

practical implementation of SINR measure is defined based on specific application purposes.

In this work SINR parameter is introduced to enable coverage calibration of FBSs in order to control overlap between adjacent femtocells. As cell radius is defined by the power of pilot signal, to achieve our goal, there is no need to calculate the appropriate SINR level of each active UE's connection. For this reason, in our simulations we do not consider RBs allocated to each UE for the SINR estimation. We measure a value that is based on pilot power signals received by each femtocell UE from its serving cell and from interfering cells. Values used in our simulations can be derived based on Reference Signal Received Power (RSRP) measurements made by UEs' which are defined by LTE specifications:

$$wSINR_u^k = \frac{RSRP_u^k}{\sum_{j=1, j \neq k}^{N+1} RSRP_u^j + N_0}, \quad (5.1)$$

where $RSRP_u^k$ is the Reference Signal Received Power (RSRP) measured by UE_u from its serving BS_k; $RSRP_u^j$ represents RSRP measured by UE_u from interfering BS_j and N_{RBs} is the total number of RBs over the E-UTRA bandwidth.

RSRP is the linear average (in watts) over the power contributions (in [W]) of the resource elements that carry cell-specific reference signals (RSs) across the channel bandwidth and is the most basic of the UE physical layer measurements. It can be calculated as:

$$RSRP_u^k = RSTPP^k - PL(d_{u,k}), \quad (5.2)$$

where $RSTP^k$ is Reference Signal Transmit Power (RSTP) (transmit power in RSs of BS_k).

6.1 The noise level on the uplink frequency band

The noise level on the uplink frequency band measured by FBS is calculated as

$$NOISE_UL_k = \sum_{u=1}^{N_u} (P_u - PL(d_{u,k})), \quad (6.1)$$

where N_u is a total number of active users in the macrocell area, P_u represents the transmit power of UE $_u$, $PL(d_{u,k})$ is a path loss between UE $_u$ and FBS $_k$.

The 3GPP specifications [18] define the setting of the UE $_u$ transmit

power by the following equation (dB scale):

$$P_u = \min(P_{max}, 10 \cdot \lg(M_u) + P_0 + \alpha \cdot PL(d_{u,j}) + \Delta_{MCS} + f(\Delta_i)), \quad (6.2)$$

where P_{max} is the maximum allowed transmit power that depends on the UE power class; M_u is the number of assigned Physical Resource Blocks (PRBs) to UE_u ; P_0 is a UE specific (optionally cell specific) parameter that represents the power allocated to one PRB; α is a cell specific path loss compensation factor; $PL(d_{u,j})$ is the downlink path loss between UE_u and its serving FBS_j , calculated in the UE_u ; Δ_{MCS} is a UE specific parameter depending on the Modulation and Coding Scheme (MCS); $f(\Delta_i)$ is a function that allows relative, cumulative and absolute corrections and it is also UE specific.

Neglecting the short term variations (Δ_{MCS} and $f(\Delta_i)$) in 6.2, the average transmit power level of UE_u becomes:

$$P_u = \min(P_{max}, 10 \cdot \lg(M_u) + P_0 + \alpha \cdot PL(d_{u,j})). \quad (6.3)$$

The path loss (in dB) is modeled based on 3GPP specifications [20] designed for urban deployment scenario.

The path loss between an indoor UE_u and the outdoor MBS is modeled as

$$PL_{NLOS}(d_{u,MBS}) = 2.7 + 42.8 \cdot \log_{10}(d_{u,MBS}) + L_{OW}, \quad (6.4)$$

where $NLOS$ denotes that there is no visual line of sight between transmitter and receiver; $d_{u,MBS}$ is a distance between UE_u and the MBS; L_{OW} is the penetration loss of an outdoor wall.

The path loss between indoor UE_u and indoor FBS_j and can be

calculated as

$$PL(d_{u,j}) = 38.46 + 20 \cdot \log 10(d_{u,j}) + 0.7 \cdot d_{2D,indoor} + 18.3 \cdot n, \quad (6.5)$$

where $(d_{u,j})$ is a distance between UE_u and the FBS_j ; $(0.7 \cdot d_{2D,indoor})$ takes account of penetration loss due to the walls inside an apartment, $d_{2D,indoor}$ is a thickness of an indoor wall and it is assumed $d_{2D,indoor} = 0.3$ [m]; n is the number of penetrated floors.

We consider a single-floor building. In this case the last term in (6.5) can be neglected.

6.2 Wideband Signal to Interference plus Noise Ratio

Each active UE_u measures the level of wideband SINR and feeds back the result to its serving FBS. This estimated value can be calculated in accordance with [21] as follows

$$wSINR_u^k = \frac{P_{r,u}^k}{I_u^k + N_0}, \quad (6.6)$$

where $P_{r,u}^k$ is the pilot power of FBS_k measured by UE_u ; I_u^k is the interference of other cells; N_0 is a thermal noise power.

Below we provide analytic expressions for calculation of the terms in (6.6).

The FBS_k pilot power measured by UE_u is modeled as

$$P_{r,u}^k = \frac{P_{t,u}^k}{A_s \cdot L_w \cdot d_{u,k}^n}, \quad (6.7)$$

where $P_{t,u}^k$ is pilot power transmitted by FBS_k and $d_{u,k}^n$ is a distance between UE_u and FBS_k.

The interference power measured by UE_u due to transmissions of all non-serving BSs (macro and femto) can be calculated as

$$I_u^k = \sum_{j=1, j \neq k}^{N+1} P_{r,u}^j, \quad (6.8)$$

where N is the total number of FBSs; $P_{r,u}^j$ is the pilot power received from interfering BS_j (calculated according to 6.7).

Note that because of “Assumption 1” of no intra-cell downlink interference, the pilot power transmitted by the serving FBS is not seen as interference by UE_u.

The FBS_k has to ensure that no UE’s $wSINR$ falls below its threshold $SINR_{TH}$ level chosen to guarantee an adequate QoS. So, the second decision-making parameter represents the minimal value of the set $\{wSINR_u^k\}$:

$$wSINR_k = \min\{wSINR_u^k\}, \forall u \in U_k, \quad (6.9)$$

where U_k is the number of active users connected to the FBS_k.

6.3 Simulation parameters

In Table 6.1 are summarized system parameters values used in simulations.

Table 6.1: *System Parameters*

| Parameter | Symbol | Value |
|-----------------------------------|--------------|-----------|
| Initial femtocell radius | R_{ini} | 7 m |
| Maximum transmit power of FBS | $P_{f,max}$ | 23 dBm |
| Minimal transmit power of FBS | $P_{f,min}$ | -40 dBm |
| Transmit power of MBS | P_t^{MBS} | 43 dBm |
| PRBs assigned to a High-Rate user | M_u | 3 |
| PRBs assigned to a Low-Rate user | M_u | 1 |
| Maximum transmit power of UEs | P_{max} | 23 dBm |
| Path loss compensation factor | α | 1 |
| Power to be contained in one PRB | P_0 | -106 dBm |
| Path loss at 1 m | A_S | 37 dBm |
| Path loss exponent | n | 3 |
| Thermal noise power | N_0 | -96.8 dBm |
| Wall penetration loss | L_{OW} | 15 dB |
| Number of FBSs | N | 5 |
| Range modification step | ΔR^+ | 2 m |
| | ΔR^- | 1 m |

CONCLUSIONS

7.1 Concluding remarks

In this dissertation, a fully distributed measurement-based coverage function for LTE FBSs embedded in a macrocell area that addresses both power consumption reduction and femto-femto interference issues is proposed.

In Chapter 4, Section 2 we have carried out a series of simulations that have permitted to set optimal values of thresholds which guarantee an optimal functioning of the algorithm (i.e. permit to achieve a trade-off between user coverage and overlapping factor of femtocells). In a low load scenario our pilot power control scheme places some FBSs in Listen Mode, that permits to reduce power consumption to up to 48.29% for each inactive femtocell. In a high load scenario each FBS dynamically adapts its pilot power (and thus the coverage) to the on-site traffic distribution and in these conditions our algorithm

allows to offload up to 13% more active users from the MBS than the static configuration scheme while guaranteeing a sufficient SINR level to all connected users. This consents not only to increase the overall system capacity, but also to improve the EE of cellular networks, as MBS's power consumption is strongly related to the traffic load.

Simulation results obtained in Chapter 4, Section 3 show that the proposed power control scheme is scalable, flexible and robust. In fact, the performance of the algorithm depends neither on the density of FBSs per unit area, nor on the MBS's location.

In Chapter 4, Section 4 we have carried out a series of simulations to determine an optimal value of ΔT , that is the time interval in which a FBS resides in Stabilization State before switching to Dynamic Power Adaption procedure. $\Delta T = 13$ [min] was chosen as an optimal value that permits to achieve a trade-off between user coverage and the number of handover events.

Furthermore, in Chapter 4, Section 5 we use a component-based model to quantify the energy saving potential of our algorithm. Simulation results show that in a case study our approach achieves an overall energy saving gain of 16.44% under a typical enterprise traffic profile.

The results obtained in in Chapter 4, Section 6 show that the proposed pilot power control scheme is suited for a Multi-MBS environment.

7.2 Possible work extensions.

7.2.1 Hybrid Access mode for Femtocells.

One of the targets of further research could be to extend the functionality of the proposed algorithm considering a "Hybrid access mode" for FBSs, in which the femtocell provides service to all UEs, but preferential treatment is given to its associated registered users, while other users can connect via a subset of remaining available subchannels on a best-effort basis.

7.2.2 Automation of setting of thresholds' values.

The performance of the proposed pilot power control scheme are strongly related to the chosen values of thresholds. More specifically, with too high *NOISE_TH* value idle FBSs would remain in Listen Mode even in the presence of active macrocell UEs located in their vicinity. This would vain the presence of FBSs. From the other side, too low *NOISE_TH* threshold level would cause useless activation of idle FBSs even when all active macrocell UEs are located outside the maximal coverage area of femtocells. This would lead to considerable energy waste and to a harmful femto-femto interference due to the overlapping between adjacent femtocells.

In this dissertation an optimal threshold's value (that permits to achieve a trade-off between percentage of users served by femtocells and overlapping factor) was determined by simulations and using specific path loss models suited for urban femtocell deployment scenario. Obviously, path loss models are good instruments, but they depend on multiple environmental factors. Obviously, the choice of optimal

NOISE_TH value depends on propagation conditions of the environment where femtocells are deployed. For example, So, the selection of some other path loss model would lead to modification of *NOISE_TH* chosen in the dissertation.

For this reason the proposed algorithm could be improved by introducing a outer loop control mechanism for automatic adaptation of threshold value to the environmental conditions where femtocells are deployed. The approach could be based on traditional retroactive schemes or on techniques of soft computing (neural networks, genetic algorithms ecc.) that learn registering activity of femtocell (useless switching on, too long Listen Mode periods ecc.) and adapt the value of threshold accordingly.

7.3 List of Publications

- [1] A. Dudnikova, D. Panno, "An energy saving approach for femtocell coverage function", Proc. 22nd ITC Specialist Seminar on Energy Efficient and Green Networking (SSEEGN), pp. 7-12, 2013.
- [2] A. Dudnikova, D. Panno, "A fully distributed algorithm for pilot power control in LTE femtocell networks", Proc. Wireless Days 2013 (WD), pp. 1-3, 2013.
- [3] A. Dudnikova, A. Mastro Simone, D. Panno, "An adaptive pilot power control approach for green heterogeneous networks", Proc. 2014 European Conference on Networks and Communications (EuCNC), pp. 1-5, June 2014.
- [4] A. Dudnikova, A. Mastro Simone, D. Panno, "A measurement-based approach for cognitive femtocell networks", Proc. 2014 European

Wireless (EW), pp. 598-603, 2014.

[5] A. Dudnikova, A. Mastro Simone, D. Panno, "Measurement-based coverage function for green femtocell networks", under major revision for publication in IEEE Computer Networks Journal.

BIBLIOGRAPHY

- [1] A. Damnjanovic, J. Montojo, Y. Wei, T. Ji, T. Luo, M. Vajapeyam, T. Yoo, O. Song, and D. Malladi, “A survey on 3gpp heterogeneous networks,” *Wireless Communications, IEEE*, vol. 18, no. 3, pp. 10–21, 2011.
- [2] V. Chandrasekhar, J. G. Andrews, and A. Gatherer, “Femtocell networks: a survey,” *Communications Magazine, IEEE*, vol. 46, no. 9, pp. 59–67, 2008.
- [3] D. Mavrakis, “Small cell market status,” Tech. Rep. 050, Informa Telecoms&Media, London, UK, Feb 2013.
- [4] H. Claussen, I. Ashraf, and L. T. Ho, “Dynamic idle mode procedures for femtocells,” *Bell Labs Technical Journal*, vol. 15, no. 2, pp. 95–116, 2010.
- [5] I. Ashraf, F. Boccardi, and L. Ho, “Sleep mode techniques for small cell deployments,” *Communications Magazine, IEEE*, vol. 49, no. 8, pp. 72–79, 2011.

-
- [6] I. Ashraf, L. T. Ho, and H. Claussen, "Improving energy efficiency of femtocell base stations via user activity detection," in *Wireless Communications and Networking Conference (WCNC), 2010 IEEE*, pp. 1–5, IEEE, 2010.
- [7] W. Li, W. Zheng, Y. Xie, and X. Wen, "Clustering based power saving algorithm for self-organized sleep mode in femto-cell networks," in *Wireless Personal Multimedia Communications (WPMC), 2012 15th International Symposium on*, pp. 379–383, IEEE, 2012.
- [8] H.-S. Jo, C. Mun, J. Moon, and J.-G. Yook, "Self-optimized coverage coordination in femtocell networks," *Wireless Communications, IEEE Transactions on*, vol. 9, no. 10, pp. 2977–2982, 2010.
- [9] I. Ashraf, H. Claussen, and L. T. Ho, "Distributed radio coverage optimization in enterprise femtocell networks," in *Communications (ICC), 2010 IEEE International Conference on*, pp. 1–6, IEEE, 2010.
- [10] S. Al-Rubaye, A. Al-Dulaimi, and J. Cosmas, "Pilot power optimization for autonomous femtocell networks," in *Wireless Advanced (WiAd), 2011*, pp. 170–175, IEEE, 2011.
- [11] M. Lin and T. La Porta, "Dynamic interference management in femtocells," in *Computer Communications and Networks (ICCCN), 2012 21st International Conference on*, pp. 1–9, IEEE, 2012.
- [12] M. Obaidat, A. Anpalagan, and I. Woungang, *Handbook of Green Information and Communication Systems*, ch. Cognitive strate-

- gies for green two-tier cellular networks, pp. 20–26. Academic Press, 1st ed. waltham ed., 2012.
- [13] S. Sesia, I. Toufik, and M. Baker, *LTE-The UMTS Long Term Evolution: From Theory to Practice*, ch. Small Signal Requirements, pp. 478–482. UK: Wiley, 2nd ed. west sussex ed., 2011.
- [14] M. Şahin, I. Guvenc, M.-R. Jeong, and H. Arslan, “Handling cci and ici in ofdma femtocell networks through frequency scheduling,” *IEEE Trans. on Consumer Electronics*, vol. 55, pp. 1936–1944, November 2009.
- [15] T.-H. Kim and T.-J. Lee, “Throughput enhancement of macro and femto networks by frequency reuse and pilot sensing,” in *Proc. IEEE International Performance, Computing and Communications Conference (IPCCC)*, pp. 390–394, Dec 2008.
- [16] P. Lee, T. Lee, J. Jeong, and J. Shin, “Interference management in lte femtocell systems using fractional frequency reuse,” in *The 12th International Conference on Advanced Communication Technology (ICACT)*, vol. 2, pp. 1047–1051, Feb 2010.
- [17] H. Claussen, L. T. W. Ho, and L. Samuel, “Self-optimization of coverage for femtocell deployments,” in *Wireless Telecommunications Symposium (WTS)*, pp. 278–285, April 2008.
- [18] “Technical specification group radio access network; evolved universal terrestrial radio access (e-utra); physical layer procedures (release 10).” 3GPP TS 36.213 v.10.0.0 Release 10, 2010.

-
- [19] G. Auer, O. Blume, V. Giannini, I. Godor, M. Imran, Y. Jading, E. Katranaras, M. Olsson, D. Sabella, P. Skillermark, *et al.*, “Energy efficiency analysis of the reference systems, areas of improvements and target breakdown,” *EARTH*, Jan 2012.
- [20] C. S. Vardhan, D. V. Ratnam, N. Bhagyasree, and A. H. Dattu, “Analysis of path loss models of 4g femtocells,” in *Wireless and Optical Communications Networks (WOCN), 2014 Eleventh International Conference on*, pp. 1–6, IEEE, 2014.
- [21] M. Simsek and A. Czystwik, *Heterogeneous Cellular Networks*, ch. Cell Selection Modes in LTE Macro–Femtocell Deployment, pp. 215–231. John Wiley & Sons Ltd, 2013.